Environment International 186 (2024) 108587

Contents lists available at ScienceDirect

Environment International

journal homepage: www.elsevier.com/locate/envint

Full length article

Global health impacts of ambient fine particulate pollution associated with climate variability

S.H.L. Yim [a,b,c,*], Y. Li [d], T. Huang [b,c], J.T. Lim [b], H.F. Lee [d], S.H. Chotirmall [b,e], G.H. Dong [f], J. Abisheganaden [b,e], J.A. Wedzicha [g], S.C. Schuster [h], B.P. Horton [a,c], J.J.Y. Sung [b]

[a] Asian School of the Environment, Nanyang Technological University, Singapore 639798, Singapore
[b] Lee Kong Chian School of Medicine, Nanyang Technological University, Singapore
[c] Earth Observatory of Singapore, Nanyang Technological University, Singapore 639798, Singapore
[d] Department of Geography and Resource Management, The Chinese University of Hong Kong, Sha Tin 999077, Hong Kong, China
[e] Department of Respiratory and Critical Care Medicine, Tan Tock Seng Hospital, Singapore
[f] Guangdong Provincial Engineering Technology Research Center of Environmental Pollution and Health Risk Assessment, Guangzhou Key Laboratory of Environmental Pollution and Health Risk Assessment, Department of Preventive Medicine, School of Public Health, Sun Yat-sen University, Guangzhou 510080, China
[g] Airways Disease Section, National Heart and Lung Institute, Imperial College London, London, UK
[h] Singapore Centre For Environmental Life Sciences Engineering (SCELSE), Nanyang Technological University, Singapore, Singapore

ARTICLE INFO

Handling Editor: Xavier Querol

Keywords:
Air pollution
Particulate matter
Health impacts
Climate variability

ABSTRACT

Air pollution is a key global environmental problem raising human health concern. It is essential to comprehensively assess the long-term characteristics of air pollution and the resultant health impacts. We first assessed the global trends of fine particulate matter ($PM_{2.5}$) during 1980–2020 using a monthly global $PM_{2.5}$ reanalysis dataset, and evaluated their association with three types of climate variability including El Niño-Southern Oscillation, Indian Ocean Dipole and North Atlantic Oscillation. We then estimated $PM_{2.5}$-attributable premature deaths using integrated exposure–response functions. Results show a significant increasing trend of ambient $PM_{2.5}$ during 1980–2020 due to increases in anthropogenic emissions. Ambient $PM_{2.5}$ caused a total of ~ 135 million premature deaths globally during the four decades. Occurrence of air pollution episodes was strongly associated with climate variability, which were associated with up to 14 % increase in annual global $PM_{2.5}$-attributable premature deaths.

1. Introduction

Air pollution is a critical environmental hazard causing significant global human health burden (Forouzanfar et al., 2016; Hong et al., 2019; Landrigan, 2017; Lelieveld et al., 2015; Romanello et al., 2022). Epidemiological studies have reported the association between air pollution and health outcomes. For example, pulmonary inflammation and an increased heart rate can be induced by exposure to fine particulate matters ($PM_{2.5}$), causing the potential development of cardiopulmonary conditions (Dockery, 2001; Donaldson et al., 2001; Gilmour et al., 2001; Pope, 2000). Also, exposure to particulate matter may lead to asthma exacerbation (Peden, 2001) and is associated to a higher risk of lung cancer, particularly adenocarcinoma of the lung (Pope et al., 2002; Yim et al., 2022). The global population-weighted $PM_{2.5}$ exposure was estimated to increase by 20.4 % led by the remarkable increase in $PM_{2.5}$ in South Asia and Southeast Asia (Brauer et al., 2016). Given the significant effects of air pollution on human health, it is essential to assess the health burden of air pollution especially under the varying anthropogenic emissions and climate.

Internal fluctuations in the mean state and other characteristics of climate, also known as climate variability, can modulate air quality through its influences on large-scale atmospheric circulations, inducing warmer and drier weather or favorable prevailing wind direction that can enhance air pollutant accumulation or transboundary air pollution, causing air pollution episodes (Bernard et al., 2001; Lin et al., 2015; Yim et al., 2019). The effects of climate variability on ambient air pollution vary in space and time (Cohen et al., 2018; Deng et al., 2021; Fasullo et al., 2018; Field et al., 2016; Franke, 2022; Le and Bae, 2022; Lorelei de Jesus et al., 2020; Mo et al., 2021; Pan et al., 2018; Pope, 2018; Reid et al., 2012; Siegert et al., 2001; Tosca et al., 2011). Recent major air

* Corresponding author at: Asian School of the Environment, Nanyang Technological University, Singapore 639798, Singapore
E-mail address: yimsteve@gmail.com (S.H.L. Yim).

https://doi.org/10.1016/j.envint.2024.108587
Received 27 December 2023; Received in revised form 18 March 2024; Accepted 18 March 2024
Available online 26 March 2024

pollution episodes have raised global concern about the effects of climate variability on air pollution such as the 2019 Australian bushfires and the most recent 2023 Canada wildfires. Spatially, El Niño and the positive phase of Indian Ocean Dipole (IOD) produced reduction in precipitation and droughts in Southeast Asia, enhancing fire emissions that further aggravated ambient air pollution (Cohen et al., 2018; Fang et al., 2024; Fasullo et al., 2018; Field et al., 2016; Franke, 2022; Gu et al., 2024; Pan et al., 2018; Reid et al., 2012; Siegert et al., 2001; Tosca et al., 2011). In contract, El Niño and positive IOD together suppressed $PM_{2.5}$ in southern part of China, inducing an increase in rainfall and a stronger southwesterly wind that enhanced air moisture (Mo et al., 2021). IOD may be associated with the abnormally high concentration of $PM_{2.5}$ in Brisbane due to the induced bushfires and dust storms, whereas the increase in $PM_{2.5}$ in Rochester and Helsinki may be due to the less precipitation led by negative North Atlantic Oscillation (NAO) during the El Niño (Lorelei de Jesus et al., 2020). The El Niño-Southern Oscillation (ENSO) influences dust concentration in Africa, America, Australia and East Asia (Le and Bae, 2022). Although previous research attempted to reveal the association between climate variability and air pollution, most of them focused on a particular kind of climate variability or a particular region. An analysis considering multiple indices simultaneously and globally is missing. Moreover, a long-term study spanning four decades can enhance our understanding of how climate variability influences air quality and public health. Given the spatial heterogeneity, a global study is required to assess the effects of different types of climate variability on air pollution, including the frequency and duration of air pollution episodes and the resultant health impacts.

This study aimed to evaluate $PM_{2.5}$ concentration and the health impact worldwide over the past four decades (1980–2020) with a particular focus on examining the association between $PM_{2.5}$ and three types of interannual climate variability including ENSO, IOD and NAO. The effects of climate variability on air quality in different regions underpin the importance and need of a global assessment study. The ground-level $PM_{2.5}$ was chosen in this study for its relevance to human health burden. In addition, the changes of the frequency and duration of air pollution episodes and the resultant human health impacts on a long-time scale require a systematic and detailed research, which is particularly important when investigating the association with climate variability.

2. Materials and methods

2.1. Grided global $PM_{2.5}$ dataset

This study collected the reanalysis data of global monthly surface $PM_{2.5}$ concentration from Modern-Era Retrospective Analysis for Research and Applications, version 2 (MERRA-2) dataset managed by the National Aeronautics and Space Administration (NASA). Compared with the previous version (MERRA-1), MERRA-2 is the latest version of global atmospheric reanalysis for the satellite era produced by NASA Global Modeling and Assimilation Office (GMAO) using the Goddard Earth Observing System Model (GEOS) version 5.12.4 (GMAO, 2015). Other applications of MERRA-2 dataset can be also found in previous work (Fang et al., 2020; Stauffer et al., 2018; Yim et al., 2022). Our collected monthly $PM_{2.5}$ dataset started from Jan 1980 to Dec 2020, at a spatial resolution of $0.5^\circ \times 0.625^\circ$.

2.2. El Niño-Southern Oscillation (ENSO), Indian Ocean Dipole (IOD), and North Atlantic Oscillation (NAO)

One of the mostly utilized ENSO indices is the Oceanic Niño Index (ONI) from NOAA. It is defined as the three-month moving mean of sea surface temperature (SST) anomaly index in Niño 3.4 region (5°N to 5°S, 150°W to 90°W). In this study, an ENSO condition was defined as a monthly ONI at or above + 1 for El Niño condition and at or below – 1 for La Niña condition during 1980 to 2020, and neutral condition was defined as $-0.5 \leq ONI \leq 0.5$. An ENSO year was defined as 5 consecutive overlapping three-month periods at or above the + 0.5° anomaly for warm (El Niño) conditions and at or below the – 0.5° anomaly for cool (La Niña) conditions. The threshold was further categorized into Weak (with a 0.5 to 0.9 SST anomaly), Moderate (1.0 to 1.4), Strong (1.5 to 1.9) and Very Strong (≥2.0) events (https://ggweather.com/enso/oni.htm, last accessed: 21 Apr 2023) (Table S1).

Monthly Dipole Mode Index (DMI) was used in this study to characterize Indian Ocean Dipole (IOD) from 1980 to 2020. The index represents the anomalous SST gradient between the western equatorial Indian Ocean (50°E-70°E and 10°S-10°N) and the southeastern equatorial Indian Ocean (90°E-110°E and 10°S-0°N), and was calculated at NOAA/PSL using the HadISST1.1 SST dataset (Ashok et al., 2001; Saji and Yamagata, 2003). Following the definition in a previous study (Hague, 2021), positive (negative) IOD conditions were identified when the three-month running mean DMI was +0.4 °C or above (– 0.4 °C or below). Neutral period was defined when the monthly DMI was situated between – 0.4 and 0.4. An IOD year was identified according to the published records from Bureau of Meteorology, Australian Government (http://www.bom.gov.au/climate/iod/, last accessed: 21 Apr 2023).

The monthly mean North Atlantic Oscillation (NAO) index was based on the surface sea-level pressure difference between the Subtropical (Azores) High and the Subpolar Low (Barnston and Livezey, 1987; van den Dool et al., 2000; Chen and den Dool, 2003). A positive (negative) value of NAO index stands for the positive (negative) phase of NAO, which is related to increased (decreased) precipitation over northern part of Europe and Scandinavia and decreased (increased) precipitation over southern and central parts of Europe. We further defined a strong positive NAO condition when the index was at or above + 0.5 and a negative NAO condition when the index was at or below – 0.5. A neutral month was identified when the index was between – 0.5 and 0.5. A NAO year was determined according to the cold season (monthly NAO index in January, February and March) average conducted by NOAA (https://www.cpc.ncep.noaa.gov/products/precip/CWlink/pna/JFM_season_nao_index.shtml, last accessed: 21 Apr 2023).

2.3. Teleconnection between global $PM_{2.5}$ concentration and climate variabilities

To distinguish the regions where the variation of air quality is subject to climate variability, teleconnections between monthly grid-based surface $PM_{2.5}$ concentration and the three climate variability indices were conducted, see Table 1. It is noted that only regions with correlation coefficients larger than 0.15 or smaller than – 0.15 and the corresponding p-values < 0.05 were selected in this study, except for ENSO where only regions with correlation coefficients larger than 0.1 or smaller than – 0.1 and corresponding p-values < 0.05 were selected. The selection of the correlation coefficients required an optimization between statistical significance and number of identified regions. We conducted a sensitivity test for the value selection and found that inclusion of regions with very small coefficients inevitably reduced the significance in the boxplot for regional comparison. Identifying too many regions may lose the focus of major vulnerable regions. So, we set the thresholds to select regions with relatively higher coefficients so that we can include as more regions as possible and exclude regions with very small coefficients at the same time.

2.4. Region classification and the definition of episodes

The regions in this study were classified according to Global Burden of Disease (GBD). To better understand the regional effect of climate variability on air quality, we further divided Africa into three sub-regions according to GBD sub-regions (Cao et al., 2022). Asia was also further divided into four sub-regions according to the classification of Asia Society (https://asiasociety.org/) (**Figure S1** and **Table S2** in Supporting Information, SI).

Table 1
Pearson correlation between each type of climate variability and $PM_{2.5}$ concentration time series.

Climate indices	Air pollution	Correlation	Interpretation	
ONI (ENSO)	$PM_{2.5}$	+	El Niño associated with high $PM_{2.5}$ concentration	La Niña associated with low $PM_{2.5}$ concentration
		–	El Niño associated with low $PM_{2.5}$ concentration	La Niña associated with high $PM_{2.5}$ concentration
DMI (IOD)	$PM_{2.5}$	+	Positive IOD phase associated with high $PM_{2.5}$ concentration	Negative IOD phase associated with low $PM_{2.5}$ concentration
		–	Positive IOD phase associated with low $PM_{2.5}$ concentration	Negative IOD phase associated with high $PM_{2.5}$ concentration
NAO	$PM_{2.5}$	+	Positive NAO phase associated with high $PM_{2.5}$ concentration	Negative NAO phase associated with low $PM_{2.5}$ concentration
		–	Positive NAO phase associated with low $PM_{2.5}$ concentration.	Negative NAO phase associated with high $PM_{2.5}$ concentration.

The identification of air pollution episode in this study was based on detrended concentration obtained by subtracting the linear trend (Callahan et al., 2019). This approach aimed to focus on the variability in the data independent of the long-term trend. An episode was considered when any of the following conditions were fulfilled:

- The average monthly $PM_{2.5}$ concentration of each region exceeded the 95th percentiles of concentration.
- The average monthly $PM_{2.5}$ concentration of each region exceeded the 75th percentiles of concentration for at least 2 consecutive months.

2.5. Health impact assessment and uncertainty

The Global Burden of Diseases, Injuries, and Risk Factors Study 2019 (GBD 2019) estimated the burden of disease attributable to 87 risk factors in 204 countries and territories from 1990 to 2019 (Murray et al., 2020). The mortality and incidence rate of each disease can be obtained in GBD 2019 through the Global Health Data Exchange (GHDx) query tool (https://ghdx.healthdata.org/gbd-results-tool), which is an online query tool of GBD 2019. Data of cases and the rates were reported as numbers with 95 % confidence intervals (C.I.). We used the AutoRegressive Integrated Moving Average (ARIMA) model to forecast the time series of diseases data to match the time range of the pollutant concentration (1980–2020). This study estimated the $PM_{2.5}$-attributable premature deaths and incidence for lower respiratory infections (LRI), tracheal, bronchus, and lung cancer, chronic obstructive pulmonary disease (COPD), stroke, and ischemic heart disease (IHD). The relative risk (RR) of each disease was calculated on the basis of criteria specified for GBD risk factors (Murray et al., 2020). It should be noted that stroke and IHD cases are rarely found in young population. GBD also provided detailed estimated RRs for different age groups for stroke and IHD according to relevant epidemiological research (Burnett et al., 2014; Danaei et al., 2006; Singh et al., 2013). Hence, in this study, people over the age of 25 were selected for the estimation of stroke and IHD, and age modification was applied to calculate the RR as described in previous epidemiological study (Burnett et al., 2014). We then applied integrated exposure–response functions (IERs) developed by Burnett el al. (2014). IERs are widely used to quantify the health impacts associated with air pollution due to their robustness. On this basis, we further enriched our analysis by incorporating an updated database from the study of Cohen et al. (2017) to estimate the global relative risk for each disease attributable to $PM_{2.5}$. This database extends the GBD dataset and integrates new RR estimates from a variety of studies conducted in different countries, providing a more comprehensive and reliable assessment of dose–response relationship between $PM_{2.5}$ exposure and health outcomes. Population-attributable fraction (PAF) was used to estimate the health outcomes E (Mansournia and Altman, 2018). The formulas are shown as follows:

$$RR(z) = 1, z < z_{fc}, \quad (1)$$

$$RR(z) = 1 + \alpha \cdot \left(1 - exp\left(- \beta \cdot \left(z - z_{fc}\right)^{\delta}\right)\right), z \geq z_{fc}, \quad (2)$$

$$E = \Sigma_k (RR_k - 1)/RR_k \cdot f_k \cdot P_k, \quad (3)$$

where z is the $PM_{2.5}$ exposure concentration; α, β, δ are parameters estimated using nonlinear regression based on the data collected; Additionally, z_{fc} is another important parameter, representing counterfactual scenario of theoretical minimum risk exposure level (TMREL) below which is assumed as no additional risk. TMREL for $PM_{2.5}$ was defined as a uniform distribution ranging from 2.4 to 5.9 μg/m^3. This range was determined based on the minimum and fifth percentiles of exposure distributions derived from outdoor air pollution cohort research (Cohen et al., 2017); If z is below the predetermined counterfactual concentration z_{fc}, it is assumed that no additional health risk is incurred, and thus RR is set to 1. In scenarios where pollution levels are exceedingly high, the risk does not increase indefinitely but is capped at a maximum value expressed as $1 + \alpha$ (Burnett et al., 2014; Chung et al., 2022). Here, α represents the scaling parameter, which determines the extent to which RR escalates once it surpasses the counterfactual threshold. The parameter β denotes the rate at which the relative risk grows with increasing $PM_{2.5}$ exposure. Meanwhile, δ represents the power of $PM_{2.5}$ concentration, predicting the risk across an extensive range of concentration, which can determine the shape of the curve relating $PM_{2.5}$ exposure to RR and affect the steepness of the RR increase; k refers to the index of the domain grid; P refers to the population size based on various population datasets; and f refers to the baseline mortality and incident rate.

Population data was estimated, validated, and interpolated based on two datasets to satisfy the study year (1980–2020). Population data after 2000 used the WorldPop Open Repository (WOPR) dataset, which provided gridded population estimates for individual countries from 2000 to 2020 at a spatial resolution of 3 arc (~100 m). Detailed methodology used to estimate the population can be found in a past study (Lloyd et al., 2019). Population data before 2000 were the result of an extension of the WOPR dataset based on Global Human Settlement Layer (GHSL) population data projections. GHSL provides global data on human population for the years 1975, 1990, 2000, and 2015, which was consisted of census data from the 2010 round of global census from Gridded Population of the World, Version 4, Revision 10 (GPWv4.10). The original data from the Joint Research Centre of the European Commission (JRC-EC) has been combined into a single data package in GeoTIFF format and reprojected from Mollweide Equal Area into WGS84 at 9 arc-second and 30 arc-second horizontal resolutions (Schiavina et al., 2019). It should be noted that the spatial resolution of the final population data was aggregated to 0.5°× 0.5° and air pollution data was resampled to the same spatial resolution based on bilinear method to fit the IERs model.

In this study, the uncertainties in air pollution estimates were derived from the MERRA-2 reanalysis data set. While the MERRA-2 dataset provides a comprehensive representation of atmospheric composition, it is inherently subject to uncertainty due to factors such as observational limitations, model resolution limitations, and potential biases in assimilated data, which are unavoidable. Therefore, we aimed to quantify the uncertainty within the IERs model by considering the variabilities in the key parameters α, β, and δ, as well as the uncertainty in the TMREL. To achieve this, we performed a Monte Carlo simulation, generating 1000 predicted IER values for each level of $PM_{2.5}$ concentration (Wu et al., 2021; Cohen et al., 2017). This simulation applied the posterior distributions for α, β, and δ—distributions that represent the

range of plausible values for these parameters as supported by epidemiological research. The TMREL was treated as a uniform distribution within the range of 2.4 to 5.9 μg/m^3, reflecting the assumption that within this range, the risk of additional adverse health effects is negligible. By integrating the posterior distributions of the parameters with the uniform distribution of TMREL, we were able to simulate a detailed uncertainty profile for the IER across varying levels of $PM_{2.5}$ exposure. The central estimate of the IER was derived from the mean of the 1000 simulations for each $PM_{2.5}$ concentration, with uncertainty defined by 95 % C.I.

3. Results

3.1. $PM_{2.5}$ level in present years and the trend during the last four decades

In terms of annual $PM_{2.5}$ concentration level in present years (2016–2020) (Fig. 1), Eastern Mediterranean (EM) and Western Sub-Saharan Africa (WSSA) were relatively higher among regions: Kuwait (122.4 μg/m^3), Niger (92.5 μg/m^3), United Arab Emirates (88.2 μg/m^3), Chad (87.5 μg/m^3) and Qatar (87.4 μg/m^3). South Asia also suffered from serious $PM_{2.5}$ pollution, i.e., Bangladesh (42.7 μg/m^3) and India (36.6 μg/m^3), followed by East Asia (EA) [China (24.5 μg/m^3) and South Korea (18.3 μg/m^3)] and Eastern Sub-Saharan Africa (ESSA) [Ethiopia (17.3 μg/m^3) and Rwanda (14.1 μg/m^3)]. Among geographical regions, North America (NA), Europe (EU) and Oceania (OC) had relatively lower $PM_{2.5}$ concentration levels in present years, i.e., the United States (8.0 μg/m^3), Greece (12.3 μg/m^3) and Australia (8.5 μg/m^3), respectively.

All the geographical regions showed a statistically significant $PM_{2.5}$ increasing trend ($p < 0.001$) except Europe and North America (Fig. 1). Among the regions, South Asia (SA) demonstrated the largest increase in $PM_{2.5}$ (0.41 μg/m^3/year), i.e., Bangladesh (0.87 μg/m^3/year) and India (0.59 μg/m^3/year). Eastern Mediterranean had the second highest $PM_{2.5}$ increasing trend i.e., Kuwait (0.60 μg/m^3/year) and Qatar (0.50 μg/m^3/year). Western Sub-Saharan Africa showed a remarkable $PM_{2.5}$ increasing trend. It notes that Senegal showed an obvious $PM_{2.5}$ declining trend (-0.27 μg/m^3/year), but it was the most polluted country (74.9 μg/m^3) in the region. Different with other regions, Europe showed an overall declining trend (-0.10 μg/m^3/year), which may be mainly due to the substantial reduction in emission of all species (**Table S3** in Supporting Information, SI). Among European countries, Romania (-0.31 μg/m^3/year) and Slovakia (-0.23 μg/m^3/year) showed the largest $PM_{2.5}$ declining trend. North America did not show any statistically significant trend.

3.2. Global air pollution episodes

3.2.1. Occurrence and duration of air pollution episodes

We defined an air pollution episode and an extreme event with detrended $PM_{2.5}$ concentration higher than its 75th and 95th percentiles, respectively. Fig. 2 shows in total 363 air pollution episodes happened around the world over the past four decades. On average, nine episodes happened in each year. The duration of an air pollution episode ranged from two to nine months. 2002 was the year with the largest number of air pollution episodes (15 episodes), followed by 2004 and 2006 (14 episodes in each of them). In these three years, all regions had at least one air pollution episode. On the contrary, 1993 was the year with the smallest number of episodes (two episodes in total): one in East Asia and one in Western Sub-Saharan Africa.

Eastern Mediterranean, Eastern Sub-Saharan Africa, and Southern Sub-Saharan Africa (SSSA) had the largest number of air pollution episodes (37 episodes in total), followed by Europe (28 episodes) and South Asia (29 episodes). Oceania had the smallest number of air pollution episodes (26 episodes in total). An air pollution episode with the longest duration (nine months) happened in Oceania in 1997 and in Southeast Asia (SEA) in 2006, whereas Oceania and Europe also had one air pollution episode with a duration of eight months in 2002 and 1989, respectively. Different with other regions, Europe showed a clear

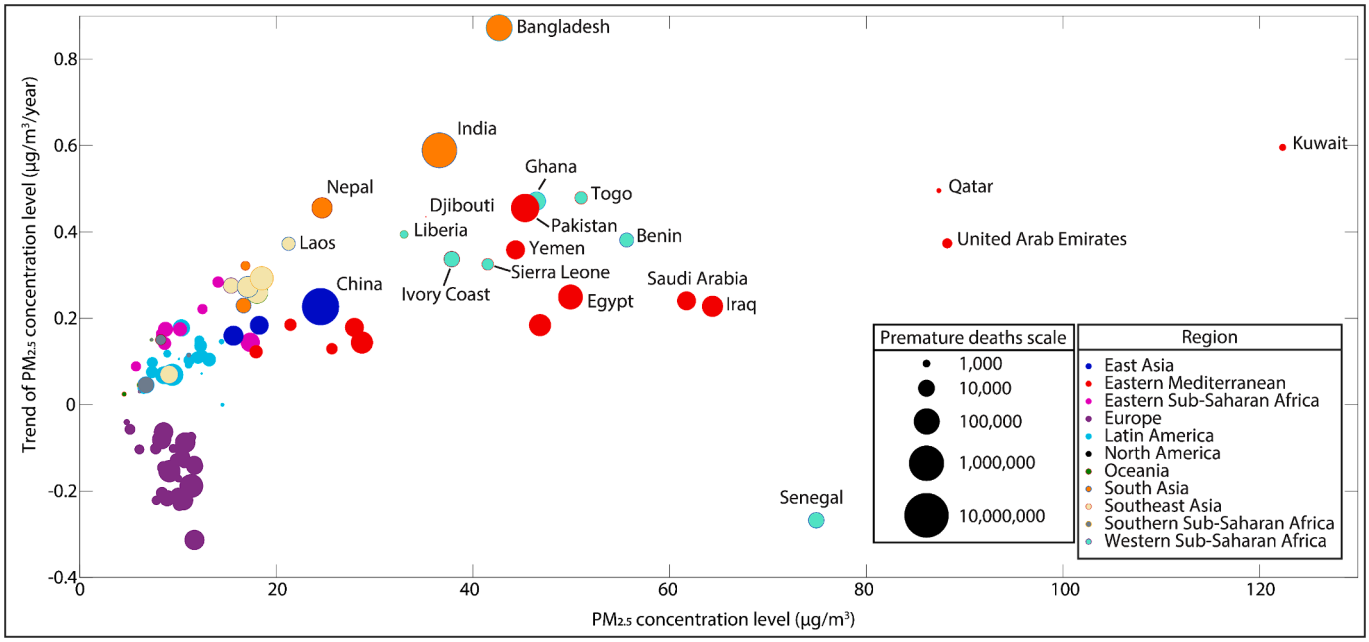

Fig. 1. The scatter plot of (x-axis) the average $PM_{2.5}$ concentration (μg/m^3) in present years (2016–2020) and (y-axis) the $PM_{2.5}$ concentration trend (μg/m^3/year) of countries from 1980 to 2020. The circle colors represent regions: East Asia (EA); Eastern Mediterranean (EM); Eastern Sub-Saharan Africa (ESSA); Europe (EU); Latin America (LA); North America (NA); Oceania (OC); South Asia (SA); Southeast Asia (SEA); Southern Sub-Saharan Africa (SSSA); Western Sub-Saharan Africa (WSSA). The size of the circles represents the average number of $PM_{2.5}$-attributable premature deaths in a year in the present years. The country names are displayed when $PM_{2.5}$ concentration is higher than 20 μg/m^3 and the trend is larger than 0.2 μg/m^3/year. The trends with p values > 0.001 were discarded. It is noted that all the North America countries had the p values > 0.001, which were considered as not statistically significant and are thus not displayed. The significance of the linear trend was evaluated using a two-tailed Student's *t* test.

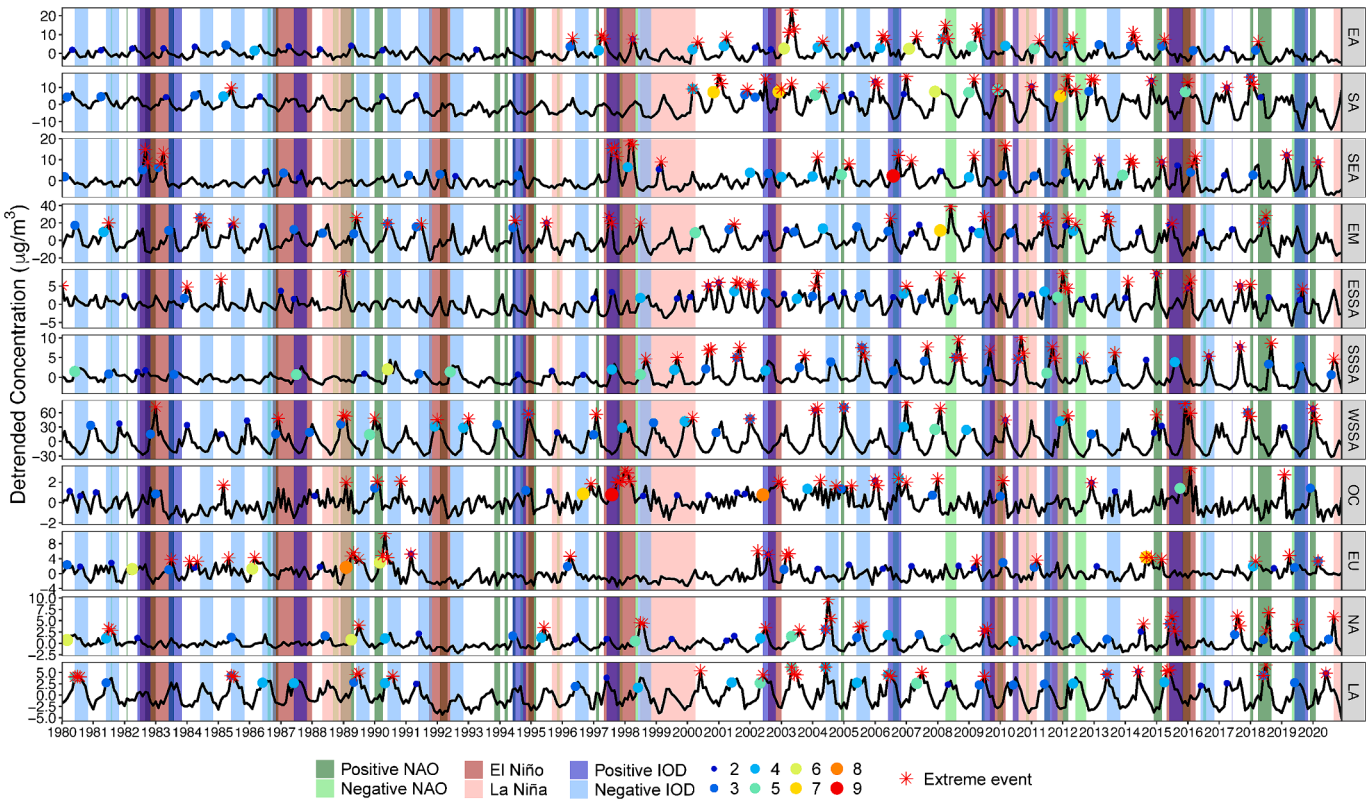

Fig. 2. The time series of detrended $PM_{2.5}$ (1980–2020) in different regions. The color columns refer to the periods of different types of climate variability including El-Niño Southern Oscillation (ENSO), Indian Ocean Dipole (IOD) and North Atlantic Oscillation (NAO). The label * refers to an extreme air pollution episode and the corresponding color dot shows the duration of the air pollution episode as swhon in the legend (unit of the duration: month).

improvement in air quality, in which air pollution episodes happened mainly in 1980 s and early 1990 s. After that period, fewer episodes with a duration longer than two months happened in Europe. In term of episodes with a short duration (two months), Eastern Sub-Saharan Africa had the largest number of episodes (25 episodes), followed by East Asia (16 episodes) and Eastern Mediterranean (15 episodes).

3.2.2. *Monthly variations of air pollution episodes*

Global monthly episode numbers varied during the past four decades (Fig. S2 and Table S4 in SI). During 1981–1990, there was a peak of number of episodes in Jun, while the minimum happened in Oct-Dec. During Jun, Eastern Mediterranean, North America, South Asia, Europe, and Latin America (LA) together contributed over 86 % of the episodes. During the low season (Oct-Dec), the episodes were dominant by Southern Sub-Saharan Africa in Oct and then by Western Sub-Saharan Africa in Nov and Dec.

This monthly profile shifted during 1991–2000, in which Aug and Sep became the peak months, whereas the minimum happened in Nov. This change was partly due to the remarkable increase in episodes in Oceania and Eastern Sub-Saharan Africa, whereas the number of episode in Western Sub-Saharan Africa reduced.

The monthly variation maintained a similar shape in 2001–2010 when compared to that in the previous decade except that the number of episodes in Mar increased remarkably and the overall number of episodes increased significantly (Fig. S2 in SI). The total number of episodes increased over 100 % in this decade when compared to that in the previous decade. South Asia and Latin America respectively increased by 487 % and 255 %, leading the increase among regions. All these findings clearly showed the serious air pollution globally in this decade.

During the fourth decade (2011–2020), the monthly variation in number of episodes became less obvious, and the global air quality had an observable improvement, especially in Jun and Mar that were the peak month in the last decade. The largest reduction in number of episodes happened in Oceania (-61 %), South Asia (-45 %) and East Asia (-42 %).

3.2.3. *Association with anthropogenic emissions*

Table S3 shows that the increasing trend of global $PM_{2.5}$ had a strong association with global anthropogenic emission trends of all the air pollutant species except sulfur dioxide (SO_2). Emissions of ammonia (NH_3) and organic carbon (OC) had a particular strong correlation as demonstrated by their large correlation coefficients of 0.86 and 0.87 ($p < 0.001$), respectively. The negative correlation coefficient −0.81, ($p < 0.001$) of SO_2 emission may be due to the complex atmospheric chemistry (Liu et al., 2018). The reduction in SO_2 emissions would reduce the formation of sulfate (SO_4^{2-}) in the atmosphere. However, the freed ammonia would then react with NO_x to form ammonium nitrate (NH_4NO_3). As a result, the reduction of SO_4^{2-} may be offset by the increase in nitrate and thus cannot be reflected in the $PM_{2.5}$ levels. This indicates the importance of controlling ammonia emissions for mitigating $PM_{2.5}$.

The result breakdown into geographical regions shows a positive correlation between the regional $PM_{2.5}$ and their emission trends in general. Some regions such as Eastern Mediterranean, South Asia or East Asia may be also affected by dust emissions in addtion to the anthropogenic ones. Fig. S3 shows that decreasing trends of dust emissions occurred in most of desert regions. This result indicates that the increases in $PM_{2.5}$ in some regions were highly associated with the increases in their anthropogenic emissions such as in East Asia, Eastern Mediterranean, Eastern Sub-Saharan Africa, South Asia, and Southern Sub-Saharan Africa. Fig. 1 shows the obvious $PM_{2.5}$ decreasing trend in Europe. It notes that the correlation between $PM_{2.5}$ in Europe and its emissions was not statistically significant even though its emissions of all species showed significant reductions. One of the possible reasons was

that the reductions in $PM_{2.5}$ in Europe may also be partly due to the reduction in transboundary air pollution in the region after the reduction in emissions (Kaldellis et al., 2007; Yim and Barrett, 2012).

3.3. Effects of climate variability on $PM_{2.5}$ concentration

In addition to anthropogenic emissions, climate variability is another important driving factor to cause or enhance air pollution episodes. Since we focused on monthly air quality, the associations between $PM_{2.5}$ and the three types of climate variability namely ENSO, IOD and NAO were analyzed. We conducted a correlation analysis between monthly time-series because even though the ENSO, IOD and NAO are interannual climate variability, most of their influences on regional air quality are shown in specific seasons (Lin et al., 2015). Moreover, annual mean time series may not necessarily represent interannual impacts because these variability conditions usually occur and last across years. Madden-Julian Oscillation was not included due to its relatively short time duration (weeks) comparing to monthly air quality.

The occurrence of air pollution episodes was strongly associated with climate variability (Fig. 2). In the year 2002, which had the largest

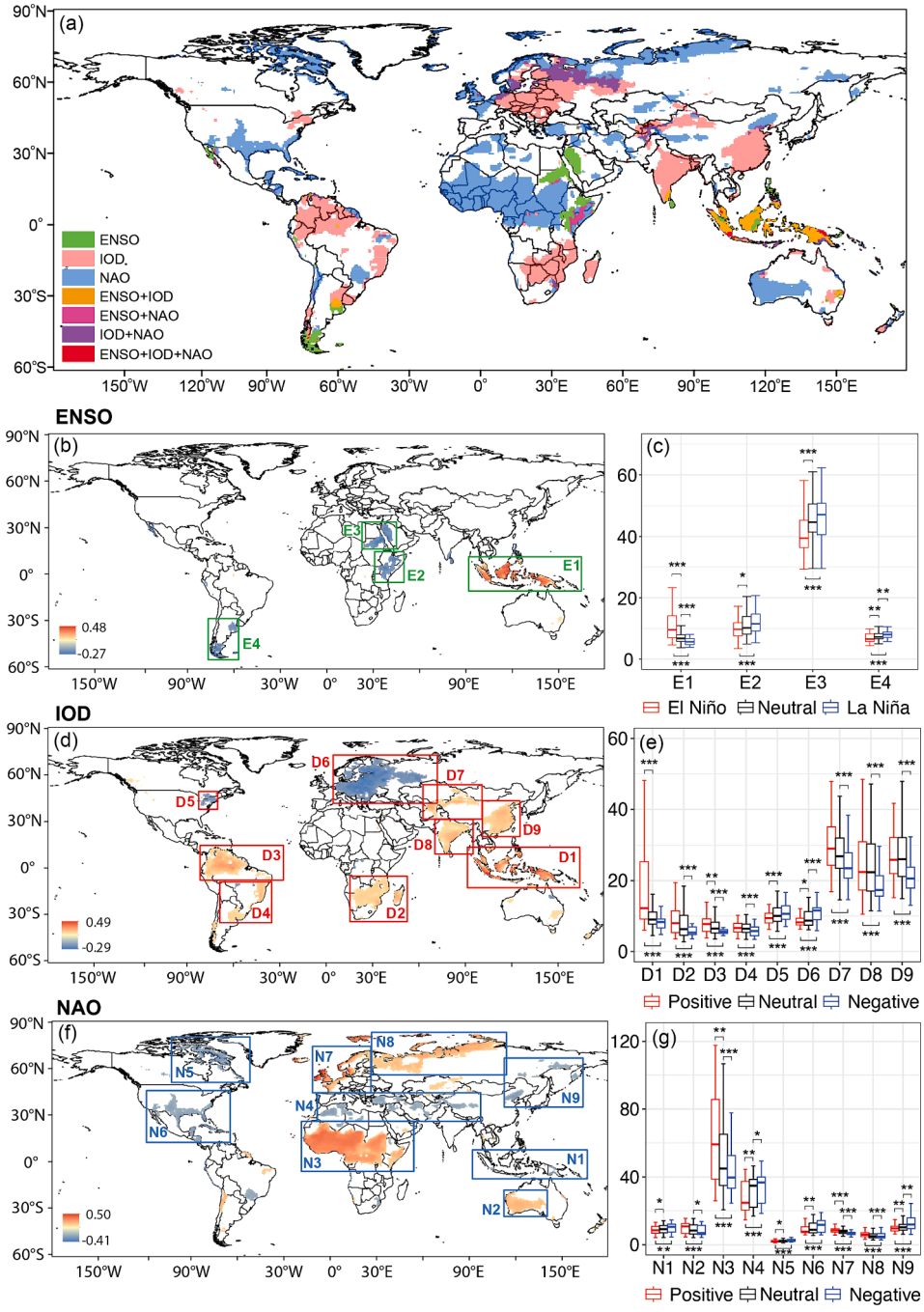

Fig. 3. The correlation between surface $PM_{2.5}$ concentration and different types of climate variability including El Niño-Southern Oscillation (ENSO), Indian Ocean Dipole (IOD) and North Atlantic Oscillation (NAO) (DJF and JJA). (a) The spatial map of the association between surface $PM_{2.5}$ concentration and each type of climate variability. Different colours represent the statistically significant association between surface $PM_{2.5}$ concentration and the corresponding type of climate variability, either individually or combined, whereas sub-figures (b), (d) and (f) focus on ENSO, IOD and NAO, respectively. The boxes show the identified areas with statistically significant associations with the corresponding box plot of the surface $PM_{2.5}$ concentration ($\mu g/m^3$) during the climate variability in the sub-figures (c), (e) and (g), respectively. The stars refer to the statistical significance (*: $p < 0.1$; **: $p < 0.05$; ***: $p < 0.01$).

number of episodes, El Niño and positive IOD happened with both positive and negative NAO. On the other hand, in 1993 with the smallest number of episodes, there was no ENSO or IOD. Regarding the longest duration of episodes identified in Oceania in 1997 and Southeast Asia in 2006 (Fig. 2), the episode in Oceania was associated with El Niño and positive IOD, whereas the one in Southeast Asia was associated with positive IOD and negative NAO. The episode with a duration of eight months in Europe was associated with La Niña and positive NAO, whereas the one in Oceania did not show any association with climate variability.

Each type of climate variability had different effects in different geographical regions (Fig. 3). Some regions even had impacts from more than one type of climate variability. For example, the maritime Southeast Asia received impacts from the three types of climate variability i.e., Perak of Malaysia and Jakarta of Indonesia. Northwestern part of Russia received the effects of both IOD and NAO, whereas East Africa received the effects of ENSO and NAO. Besides these three regions, other commonly affected regions may receive effects from only one individual type of climate variability, such as the effect of ENSO in the Eastern Sub-Saharan Africa and the most southern part of Latin America, the effect of IOD in continental Europe, China and India, and the effect of NAO in the central part of Africa and the western part of Australia.

Surface $PM_{2.5}$ concentration levels changed under the influence of different types of climate variability. Four subregions were identified based on their statistically significant correlation between surface $PM_{2.5}$ concentration and the ENSO winters (Fig. 3**b**). El Niño and La Niña had varying effects on surface $PM_{2.5}$ concentration (Fig. 3**c**). The effect of ENSO in maritime Southeast Asia (E1) was remarkable. The regional surface $PM_{2.5}$ concentration was 124 % higher in El Niño winters than in neutral winters, whereas it was 19 % lower in La Niña winters than in neutral winters. The opposite situation happened in East Africa (E2 & E3) and southern part of Latin America (E4). In which, the surface $PM_{2.5}$ concentration was 8–11 % lower in El Niño winter and 2–11 % higher in La Niña winters when comparing with that in neutral winters.

Fig. 3**d&e** demonstrate the significant association between IOD and $PM_{2.5}$ levels. Nine subregions were identified to show strong correlation: four in Southeast Asia, one in Europe, one in Southern Sub-Saharan Africa, one in North America and two in Latin America. The results show that $PM_{2.5}$ was (mean: 3–114 %) higher with positive IOD but (mean: 4–28 %) lower with negative IOD in Southeast Asia (D1), South Africa (D2), northern part of South America (D3), eastern part of South America (D4), northwestern part of Asia (D7) and South Asia (D8). Nevertheless, this situation reversed in northeastern part of the United States (D5) and Europe (D6), in which, when comparing with the neutral situation, $PM_{2.5}$ was (5–18 %) higher with negative IOD and (8–9 %) lower in positive IOD.

The effect of NAO was reflected in Fig. 3**c**. In total, nine subregions were identified based on the strong correlation between $PM_{2.5}$ and NAO. Positive NAO was associated with higher $PM_{2.5}$ levels (mean 9–21 %) but lower $PM_{2.5}$ levels (mean 5–14 %) in western and southern parts of Australia (N2), central part of Africa (N3), western part of Europe (N7) and northern part of Russia (N8). On the contrary, negative associations between NAO and $PM_{2.5}$ levels were found in maritime Southeast Asia (N1), North Africa and Middle East (N4), northern part of Canada (N5), southern part of the United States (N6) and some areas in northeastern part of China and eastern part of Russia (N9), in which $PM_{2.5}$ was (mean: 9–19 %) higher with negative NAO but (mean: 3–12 %) lower with positive NAO relative to the neutral situation.

Our results show the significant spatial variation of climate variability impacts on $PM_{2.5}$ levels. It should be highlighted that the Maritime Continent of Southeast Asia is the region of the world that had statistically significant effects of ENSO, IOD and NAO on its surface $PM_{2.5}$ concentration together. As shown in our results, the $PM_{2.5}$ concentration in the Maritime Continent was higher in El Niño winter, positive IOD and negative NAO.

3.4. Health impact assessment

3.4.1. Health impact due to $PM_{2.5}$ exposure

Applying integrated exposure–response functions (IERs) developed by previous epidemiological studies (Burnett et al., 2014; Cohen et al., 2017), we estimated that outdoor $PM_{2.5}$ pollution caused a total of ~ 135 million of premature deaths globally from 1980 to 2020. Among the conditions, stroke and ischemic heart disease (IHD) were the main diseases accounting for 33.3 % and 32.7 %, respectively, followed by COPD (15.5 %), LRI (11.9 %) and lung cancer (6.7 %). We compared our results with the results reported by World Health Organization (WHO) and other published papers according to their reported years, see **Table S5** in SI. The comparison shows that majority of their results are within our uncertainty ranges. Although some may not fall into the range, their values are not too different with ours. This confirmed the robustness of our results.

Among regions, Asia was estimated to have the largest number of $PM_{2.5}$-attributable premature deaths [98.1 (C.I.: 65.5–125.0) million] from 1980 to 2020 (Fig. 4). In Asia, China and India had the highest number of $PM_{2.5}$-attributable premature deaths, accounting for 49.0 (C.I.: 33.8–61.5) million and 26.1 (C.I.: 17.5–33.1) million, respectively. Besides the two countries, Pakistan, Bangladesh, Indonesia, and Japan had a remarkable number of $PM_{2.5}$-attributable premature deaths, ranging from 2 to 5 million in each of them.

Africa [16.2 (C.I.: 10.4–21.1) million] and Europe [15.8 (C.I.: 6.6–23.5) million] were ranked as the second and third regions in term of $PM_{2.5}$- attributable premature deaths, respectively. In Africa, the number of premature deaths was outstanding in Nigeria [4.4 (C.I.: 3.1–5.4) million], Egypt [2.3 (C.I.: 1.6–2.8) million] and Sudan [1.4 (C.I.: 1.0–1.7) million]. In Europe, six countries particularly dominated, including Ukraine [2.7 (C.I.: 1.2–3.9) million], Germany [2.3 (C.I.: 0.9–3.5) million], Poland [1.3 (C.I.: 0.6–1.8) million], the United Kingdom [1.2 (C.I.: 0.4–2.0) million], Romania [1.1 (C.I.: 0.6–1.6) million] and Italy [1.1 (C.I.: 0.5–1.7) million]. Their $PM_{2.5}$-attributable premature deaths when combined accounted for 62 % of the total $PM_{2.5}$-attributable premature deaths in Europe.

The Americas had 5.0 (C.I.: 1.5–8.0) million $PM_{2.5}$-attributable premature deaths in total, of which 46 % were in North America. In North America, the United States dominated the impact, accounting for more than 78 % of the total premature deaths in North America. In Latin America, Brazil showed the most prominent health impact [1.1 (C.I.: 0.2–1.8) million], 78 % more $PM_{2.5}$-attributable premature deaths than that in Mexico [0.6 (C.I.: 0.2–0.9) million], which is the country with the second highest $PM_{2.5}$-attributable premature deaths. This reflects the serious adverse air pollution problem in Brazil. Oceania had the least $PM_{2.5}$-attributable premature deaths, accounting for 0.2 (C.I.: 0.0–0.4) million, mainly happening in Australia [0.2 (C.I.: 0.0–0.3) million].

3.4.2. Health impact due to $PM_{2.5}$ exposure under the influence of climate variability

The changes in annual $PM_{2.5}$-attributable premature deaths associated with various types of climate variability are shown (Fig. 5). The estimations were based on the changes of annual $PM_{2.5}$-attributable premature deaths in the identified regions with a statistically significant association between $PM_{2.5}$ and each type of climate variability. Our estimations show that an increase of ~ 1,400 annual $PM_{2.5}$-attributable premature deaths was associated with El Niño when comparing with those in neutral years. The larger number of annual $PM_{2.5}$-attributable premature deaths mainly occurred in Southeast Asia (E1). On the contrary, ~350 annual $PM_{2.5}$-attributable premature deaths due to $PM_{2.5}$ were avoided due to La Niña when comparing with those in neutral years.

Positive IOD was estimated to associate with 3,100 more annual $PM_{2.5}$-attributable premature deaths comparing with neutral years, whereas a reduction of ~ 23,000 annual $PM_{2.5}$-attributable premature deaths were associated with negative IOD. The largest effect of positive

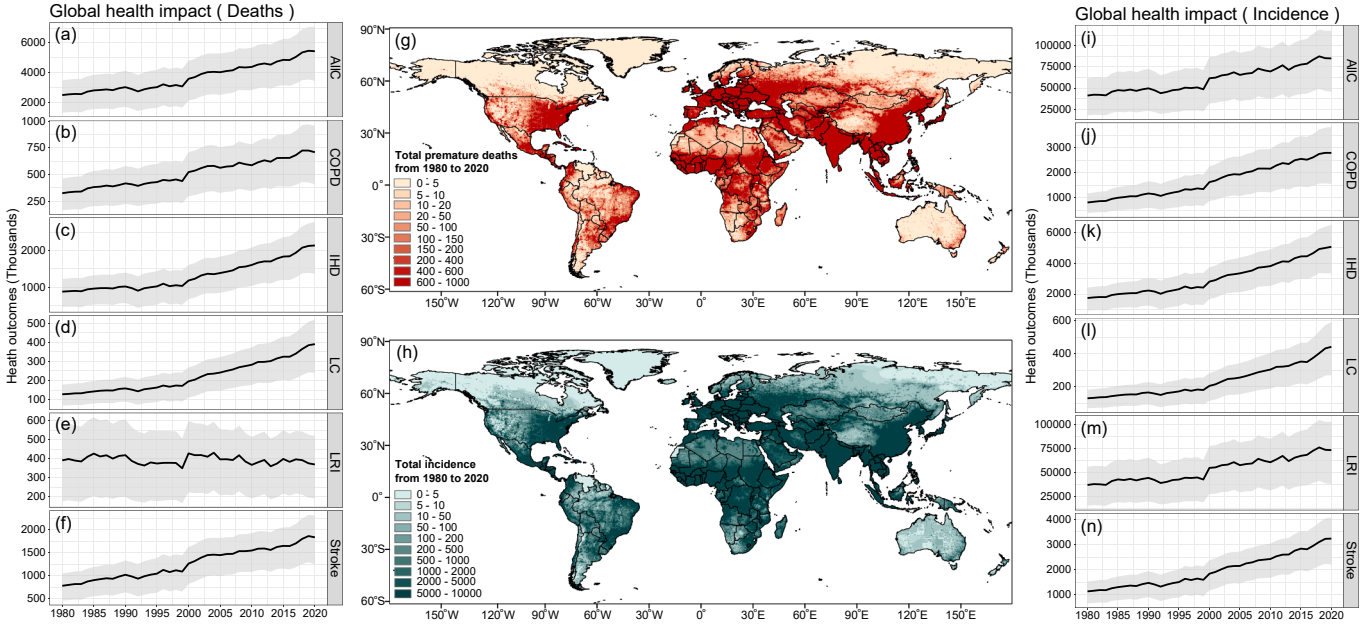

Fig. 4. The total $PM_{2.5}$-attributable (a-f and g) premature deaths and (h, i-n) incidence in different countries during 1980–2020. (a-f) are the time series of $PM_{2.5}$-attributable premature deaths for (a) all causes, (b) chronic obstructive pulmonary disease (COPD), (c) ischemic heart disease (IHD), (d) lung cancer (LC), (e) lower respiratory infection (LRI), and (f) stroke, whereas (i-n) are the same as (a-f) but for incidence. The shaded areas in gray color in (a-f and i-n) represent the uncertainty ranges at 95 confidence intervals (C.I.).

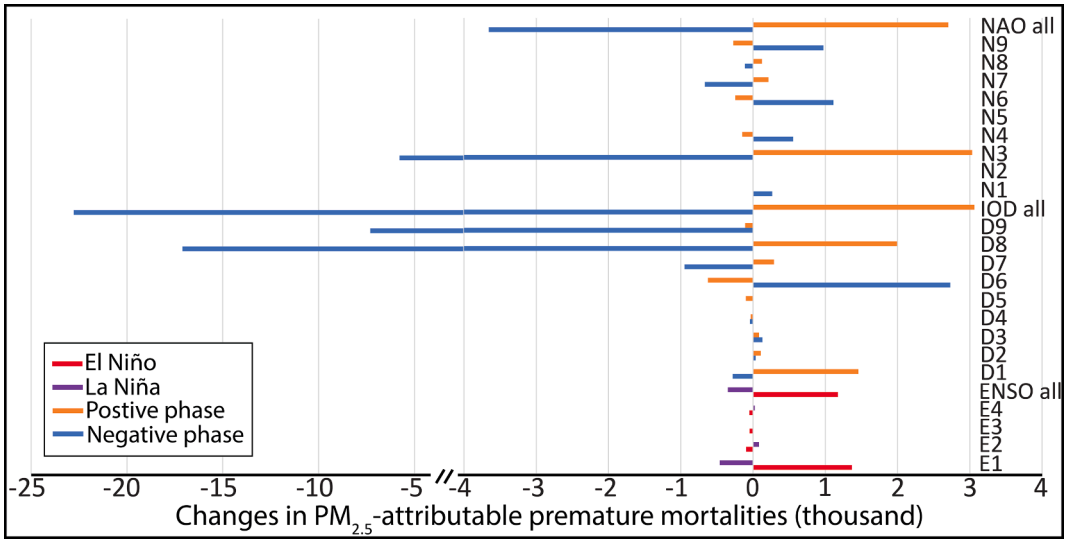

Fig. 5. The estimated changes in annual $PM_{2.5}$-attributable premature deaths per year associated with each type of climate variability. The domains are referred to Fig. 3. Red bars represent El Niño, whereas purple bars are La Niña; For IOD and NAO, orange bars represent a positive phase, while blue bars represent a negative phase. (For interpretation of the references to color in this figure legend, the reader is referred to the web version of this article.)

IOD associated with an increase in annual $PM_{2.5}$-attributable premature deaths occurred in South Asia (mainly in India) (D8) (~2,000) and Southeast Asia (D1) (~1,500), followed by northwestern part of China (D7) (~290). For negative IOD, the largest number of avoided annual $PM_{2.5}$-attributable premature deaths happened in South Asia (mainly in India) (D8) (~17,000) followed by East Asia (D9) (~7,300).

Positive NAO was estimated to associate with an increase of ~ 2,700 annual $PM_{2.5}$-attributable premature deaths comparing with neutral years, whereas negative NAO showed ~ 3,700 less. The large effect for the positive NAO associated with an increase in annual $PM_{2.5}$-attributable premature deaths occurred in northern part of Russia (N8) (~120), and central part of Africa and southern part of Western Sub-Saharan Africa (N3) (~3,000). The increase in annual $PM_{2.5}$-attributable premature deaths associated with the effect of negative NAO mainly occurred in southern part of North America (mainly in the United States) (N6) (~1,100) followed by northern part of Africa and Middle East (N4) (~560) and Southeast Asia (N1) (~270).

We estimated that an increase of ~ 7,000 global annual $PM_{2.5}$-attributable premature deaths were associated with El Niño, positive IOD and positive NAO together. In the four decades of our studied period, 1994, 1997, 2002 and 2015 were the four years with such combination of the three types of climate variability in a year. Southeast Asia was found to be particularly susceptive to the three types of climate variability as shown by the 3,100 additional annual $PM_{2.5}$-attributable premature deaths in the region due to the three studied types of climate variability. On the other hand, a year under the effect of La Niña,

negative IOD and negative NAO may be associated with better global air quality. Nevertheless, the long-term record did not show this combination during the past four decades.

4. Discussion and implications

This study comprehensively analyzed $PM_{2.5}$ pollution and the health impacts over the past four decades. Our results clearly show the adverse human health impact of $PM_{2.5}$ pollution particularly related to cardiopulmonary conditions and strokes. There was also a modest increase in lung cancer related to the effect of air pollution. The obvious increase trend in $PM_{2.5}$-attributable premature deaths indicates the urgency and importance to control air pollution to mitigate human health impacts. In developing countries where air pollution is serious, their air quality management typically focuses on reducing air pollutant concentration levels. Limited attention has been paid on employing the health benefit as one of the criteria in the formulation of emission control policies and strategies in the developing countries. This study emphasizes the significance of health-oriented air quality strategies in air quality management. When governments evaluate environmental policies, their focus should not be only on air pollutant levels but also on the health outcomes. Environmental evaluation should assess the effectiveness of emission control policy on the reduction in air pollution-related health outcomes. Moreover, given the serious human health impact of $PM_{2.5}$ pollution, health-related agencies should allocate more resources to fulfill the healthcare demands due to $PM_{2.5}$ pollution.

The association of climate variability with air quality and the resultant health impacts is one of the focuses of this study. Our results show that global air quality became the worst when El Niño, positive IOD and positive NAO happened simultaneously, inducing frequent air pollution episodes across five continents. Although the $PM_{2.5}$-attributable premature deaths associated with climate variability were not comparable with the overall $PM_{2.5}$-attributable premature deaths, our study demonstrated the influences on global scale and highlighted regions vulnerable to multiple types of climate variability. For example, Southeast Asia was susceptive to the effects of El Niño, positive IOD and positive NAO. Southeast Asia has been undergoing rapid urbanization (Arfanuzzaman and Dahiya, 2019; Behera and Dash, 2017), industrialization with substantial anthropogenic emissions (Ohara et al., 2007), i.e. substantial biomass burning activities, unsustainable land-use planning, environmental quality degradation, large amount of population and large ecological footprints (Arfanuzzaman and Dahiya, 2019). Southeast Asia was also reported to have an increase trend in $PM_{2.5}$ pollution, leading the global increasing trend (Brauer et al., 2016). While the region experiences all these human and environmental factors, the remarkable effects of climate variability would further worsen the problems in the region. Nevertheless, Southeast Asia could also be a test-bed for new and innovative solutions to mitigate the effects of air quality on population health. Furthermore, given the impacts of climate variability on air quality, effectiveness of emission control policies may be significantly reduced if climate variability is not considered. This study hence suggests a stricter emission control strategy to offset the enhancement of large-scale oscillations on air pollution due to climate variability.

This study provides critical information for identifying vulnerability in term of air pollution-related health impacts to reduce air pollution exposure and vulnerabilities, and to increase global population health resilience. Nevertheless, there exist some limitations. Our analysis uses the global data for four decades with a spatial resolution that may not fully reflect air pollution on local scale. More research should be done when finer spatial $PM_{2.5}$ data is available. Despite the robustness of our results, the number of air pollution episodes may vary with different thresholds. In-depth studies should be done in each city for better understanding local air pollution episode characteristics. This study provides an insight of the association between $PM_{2.5}$ pollution and climate variability. Nevertheless, more investigations are still required to understand the processes of how climate variability affects $PM_{2.5}$ formation and removal, and to further understand the influence of short-term climate variability, e.g., Madden Julian Oscillation (MJO) on $PM_{2.5}$ pollution around the world. Furthermore, this study mainly focused on the exposure of ambient $PM_{2.5}$, while exposure of indoor $PM_{2.5}$ and other air pollutants are also a critical source of human health impact due to air pollution. This would need further research to evaluate the effect in detail. In addition, the non-linear effects between the three studied types of climate variability have not yet been assessed, and require in-depth investigations. It should also be noted that the toxicity effect may vary among $PM_{2.5}$ species. Our health assessment assumed the same toxicity for various species due to lack of detailed information about the toxicity effects of different $PM_{2.5}$ species. This should be improved when more data is available.

CRediT authorship contribution statement

S.H.L. Yim: Writing – original draft, Visualization, Validation, Supervision, Software, Resources, Methodology, Investigation, Formal analysis, Conceptualization. **Y. Li:** Writing – review & editing, Visualization, Validation, Software, Methodology, Investigation, Formal analysis. **T. Huang:** Writing – review & editing, Visualization, Validation, Software, Methodology, Investigation, Formal analysis. **J.T. Lim:** Writing – review & editing. **H.F. Lee:** Writing – review & editing, Formal analysis. **S.H. Chotirmall:** Writing – review & editing, Formal analysis. **G.H. Dong:** Writing – review & editing, Formal analysis. **J. Abisheganaden:** Writing – review & editing, Formal analysis. **J.A. Wedzicha:** Writing – review & editing, Formal analysis. **S.C. Schuster:** Writing – review & editing, Formal analysis. **B.P. Horton:** Writing – review & editing, Formal analysis. **J.J.Y. Sung:** Writing – review & editing, Formal analysis.

Declaration of competing interest

The authors declare that they have no known competing financial interests or personal relationships that could have appeared to influence the work reported in this paper.

Data availability

Data will be made available on request.

Acknowledgement

This research is jointly supported by the Ministry of Education, Singapore, under its MOE AcRF Tier 3 Award MOET32022-0006, Start-up Grant from NTU (SUG: 021384-00001) and Ministry of Education of Singapore (MOE SUG: 021452-00001), MOE AcRF Tier 1 from Ministry of Education of Singapore (RG126/21: 021591-00001), EOS FY2022 funding (EOS MOE RCE FY 2022: 021943-0001) from Earth Observatory of Singapore at NTU, The Prudential EOS Climate Impacts Initiative by Prudential Services Singapore Pte. Ltd. (022834-00001) and Dr. Stanley Ho Medical Development Foundation (grant no. 8305509). This work comprises EOS contribution number 583.

Appendix A. Supplementary material

Supplementary data to this article can be found online at https://doi.org/10.1016/j.envint.2024.108587.

References

Arfanuzzaman, Md., Dahiya, B., 2019. Sustainable urbanization in Southeast Asia and beyond: Challenges of population growth, land use change, and environmental health. Growth Chang. 50, 725–744.

Ashok, K., Guan, Z., Yamagata, T., 2001. Impact of the Indian Ocean dipole on the relationship between the Indian monsoon rainfall and ENSO. Geophys. Res. Lett. 28, 4499–4502.
Barnston, A.G., Livezey, R.E., 1987. Classification, seasonality and persistence of low-frequency atmospheric circulation patterns. Mon. Weather Rev. 115, 1083–1126.
Behera, S.R., Dash, D.P., 2017. The effect of urbanization, energy consumption, and foreign direct investment on the carbon dioxide emission in the SSEA (South and Southeast Asian) region. Renew. Sustain. Energy Rev. 70, 96–106.
Bernard, S.M., Samet, J.M., Grambsch, A., Ebi, K.L., Romieu, I., 2001. The potential impacts of climate variability and change on air pollution-related health effects in the United States. Environ. Health Perspect. 109, 199–209.
Burnett, R.T., Pope, C.A., Ezzati, M., Olives, C., Lim, S.S., Mehta, S., Shin, H.H., Singh, G., Hubbell, B., Brauer, M., Anderson, H.R., Smith, K.R., Balmes, J.R., Bruce, N.G., Kan, H., Laden, F., Prüss-Ustün, A., Turner, M.C., Gapstur, S.M., Diver, W.R., Cohen, A., 2014. An Integrated Risk Function for Estimating the Global Burden of Disease Attributable to Ambient Fine Particulate Matter Exposure. Environmental Health Perspectives 122, 397–403.
Callahan, C.W., Schnell, J.L., Horton, D.E., 2019. Multi-index attribution of extreme winter air quality in Beijing, China. J. Geophys. Res.: Atmos. 124, 4567–4583.
Cao, H., Cao, X., Cao, Z., Zhang, L., Han, Y., Guo, C., 2022. The prevalence and causes of pediatric uncorrected refractive error: Pooled data from population studies for Global Burden of Disease (GBD) sub-regions. PLOS ONE 17, e0268800.
Chen, W.Y., den Dool, H.V., 2003. Sensitivity of teleconnection patterns to the sign of their primary action center. Mon. Weather Rev. 131, 2885–2899.
Chung, C.Y., Yang, J., Yang, X., He, J., 2022. Mathematical modeling in the health risk assessment of air pollution-related disease burden in China: a review. Front. Public Health 10.
Cohen, J.B., Ng, D.H.L., Lim, A.W.L., Chua, X.R., 2018. Vertical distribution of aerosols over the Maritime Continent during El Niño. Atmos. Chem. Phys. 18, 7095–7108.
Danaei, G., Lawes, C.M., Vander Hoorn, S., Murray, C.J., Ezzati, M., 2006. Global and regional mortality from ischaemic heart disease and stroke attributable to higher-than-optimum blood glucose concentration: comparative risk assessment. Lancet 368, 1651–1659.
Deng, W., Cohen, J.B., Wang, S., Lin, C., 2021. Improving the understanding between climate variability and observed extremes of global NO2 over the past 15 years. Environ. Res. Lett. 16, 054020.
Dockery, D.W., 2001. Epidemiologic evidence of cardiovascular effects of particulate air pollution. Environ. Health Perspect. 109, 483–486.
Donaldson, K., Stone, V., Seaton, A., MacNee, W., 2001. Ambient particle inhalation and the cardiovascular system: potential mechanisms. Environ Health Perspect 109 (Suppl 4), 523–527.
Yim, S.H.L., Huang, T., Ho, J.M.W., Lam, A.S.M., Yau, S.T.Y., Yuen, T.W.H., Dong, G.H., Tsoi, K.K.F., Sung, J.J.Y., 2022. Rise and fall of lung cancers in relation to tobacco smoking and air pollution: A global trend analysis from 1990 to 2012. Atmos. Environ. 269, 118835.
Cohen, A.J., Brauer, M., Burnett, R., Anderson, H.R., Frostad, J., Estep, K., Balakrishnan, K., Brunekreef, B., Dandona, L., Dandona, R., Feigin, V., Freedman, G., Hubbell, B., Jobling, A., Kan, H., Knibbs, L., Liu, Y., Martin, R., Morawska, L., Pope, C.A., Shin, H., Straif, K., Shaddick, G., Thomas, M., Dingenen, R. van, Donkelaar, A. van, Vos, T., Murray, C.J.L., Forouzanfar, M.H., 2017. Estimates and 25-year trends of the global burden of disease attributable to ambient air pollution: an analysis of data from the Global Burden of Diseases Study 2015. The Lancet 389, 1907–1918.
Brauer, M., Freedman, G., Frostad, J., van Donkelaar, A., Martin, R.V., Dentener, F., Dingenen, R. van, Estep, K., Amini, H., Apte, J.S., Balakrishnan, K., Barregard, L., Broday, D., Feigin, V., Ghosh, S., Hopke, P.K., Knibbs, L.D., Kokubo, Y., Liu, Y., Ma, S., Morawska, L., Sangrador, J.L.T., Shaddick, G., Anderson, H.R., Vos, T., Forouzanfar, M.H., Burnett, R.T., Cohen, A., 2016. Ambient Air Pollution Exposure Estimation for the Global Burden of Disease 2013. Environ. Sci. Technol. 50, 79–88.
Fang, T., Gu, Y., Yim, S.H.L., 2024. Assessing local and transboundary fine particulate matter pollution and sectoral contributions in Southeast Asia during haze months of 2015–2019. Sci. Total Environ. 912, 169051.
Fang, C., Zhu, B., Pan, C., Yun, X., Ding, D., Tao, S., 2020. Regional and Sectoral Sources for Black Carbon Over South China in Spring and Their Sensitivity to East Asian Summer Monsoon Onset. J. Geophys. Res.-Atmos 125 e2020JD033219.
Fasullo, J.T., Otto-Bliesner, B.L., Stevenson, S., 2018. ENSO's Changing Influence on Temperature, Precipitation, and Wildfire in a Warming Climate. Geophys. Res. Lett. 45, 9216–9225.
Field, R.D., van der Werf, G.R., Fanin, T., Fetzer, E.J., Fuller, R., Jethva, H., Levy, R., Livesey, N.J., Luo, M., Torres, O., Worden, H.M., 2016. Indonesian fire activity and smoke pollution in 2015 show persistent nonlinear sensitivity to El Niño-induced drought. Proc. Natl. Acad. Sci. 113, 9204–9209.
Forouzanfar, M.H., et al., 2016. Global, regional, and national comparative risk assessment of 79 behavioural, environmental and occupational, and metabolic risks or clusters of risks, 1990–2015: a systematic analysis for the Global Burden of Disease Study 2015. Lancet 388, 1659–1724.
Franke, J., 2022. El Niño enhances wildfire emissions. Nat. Clim. Chang. 12, 964.
Gilmour, M.I., Daniels, M., McCrillis, R.C., Winsett, D., Selgrade, M.K., 2001. Air pollutant-enhanced respiratory disease in experimental animals. Environ. Health Perspect. 109, 619–622.
Gu, Y., Fang, T., Yim, S.H.L., 2024. Source Emission Contributions to Particulate Matter and Ozone, and Their Health Impacts in Southeast Asia. Environ. Int. 186, 108578.
Hague, B.S., 2021. Seasonal climate summary for Australia and the southern hemisphere (summer 2018–19): extreme heat and flooding prominent. JSHESS 71, 147–158.
Hong, C., Zhang, Q., Zhang, Y., Davis, S.J., Tong, D., Zheng, Y., Liu, Z., Guan, D., He, K., Schellnhuber, H.J., 2019. Impacts of climate change on future air quality and human health in China. Proc. Natl. Acad. Sci. 116, 17193–17200.
Kaldellis, J.K., Chalvatzis, K.J., Spyropoulos, G.C., 2007. Transboundary air pollution balance in the new integrated European environment. Environ. Sci. Pol. 10, 725–733.
Landrigan, P.J., 2017. Air pollution and health. Lancet Public Health 2, e4–e5.
Le, T., Bae, D.-H., 2022. Causal influences of El Niño-Southern Oscillation on global dust activities. Atmos. Chem. Phys. 22, 5253–5263.
Lelieveld, J., Evans, J.S., Fnais, M., Giannadaki, D., Pozzer, A., 2015. The contribution of outdoor air pollution sources to premature mortality on a global scale. Nature 525, 367–371.
Lin, M., Fiore, A.M., Horowitz, L.W., Langford, A.O., Oltmans, S.J., Tarasick, D., Rieder, H.E., 2015. Climate variability modulates western US ozone air quality in spring via deep stratospheric intrusions. Nat Commun 6, 7105.
Liu, M., Huang, X., Song, Y., Xu, T., Wang, S., Wu, Z., Hu, M., Zhang, L., Zhang, Q., Pan, Y., Liu, X., Zhu, T., 2018. Rapid SO_2 emission reductions significantly increase tropospheric ammonia concentrations over the North China Plain. Atmos. Chem. Phys. 18, 17933–17943.
Lloyd, C.T., Chamberlain, H., Kerr, D., Yetman, G., Pistolesi, L., Stevens, F.R., Gaughan, A.E., Nieves, J.J., Hornby, G., MacManus, K., Sinha, P., Bondarenko, M., Sorichetta, A., Tatem, A.J., 2019. Global spatio-temporally harmonised datasets for producing high-resolution gridded population distribution datasets. Big Earth Data 3, 108–139.
Lorelei de Jesus, A., Thompson, H., Knibbs, L.D., Kowalski, M., Cyrys, J., Niemi, J.V., Kousa, A., Timonen, H., Luoma, K., Petäjä, T., Beddows, D., Harrison, R.M., Hopke, P., Morawska, L., 2020. Long-term trends in PM2.5 mass and particle number concentrations in urban air: The impacts of mitigation measures and extreme events due to changing climates. Environ. Poll. 263, 114500.
Mansournia, M.A., Altman, D.G., 2018. Population attributable fraction. BMJ 360, k757.
Mo, H., Liu, R., Liu, S.C., Mo, J., 2021. Synergetic effect of El Niño-Southern Oscillation and Indian Ocean Dipole on particulate matter in Guangdong, China. Int. J. Climatol. 41, 3615–3627.
Murray, C.J.L., et al., 2020. Global burden of 87 risk factors in 204 countries and territories, 1990–2019: a systematic analysis for the Global Burden of Disease Study 2019. Lancet 396, 1223–1249.
Ohara, T., Akimoto, H., Kurokawa, J., Horii, N., Yamaji, K., Yan, X., Hayasaka, T., 2007. An Asian emission inventory of anthropogenic emission sources for the period 1980–2020. Atmos. Chem. Phys. 7, 4419–4444.
Pan, X., Chin, M., Ichoku, C.M., Field, R.D., 2018. Connecting Indonesian Fires and Drought With the Type of El Niño and Phase of the Indian Ocean Dipole During 1979–2016. J. Geophys. Res. Atmos. 123, 7974–7988.
Peden, D.B., 2001. Air pollution in asthma: effect of pollutants on airway inflammation. Ann Allergy Asthma Immunol 87, 12–17.
Pope, R.J., et al., 2018. Influence of the wintertime North Atlantic Oscillation on European tropospheric composition: an observational and modelling study. Atmos. Chem. Phys. 18, 8389–8408.
Pope III, C.A., Burnett, R.T., Thun, M.J., Calle, E.E., Krewski, D., Ito, K., Thurston, G.D., 2002. Lung Cancer, Cardiopulmonary Mortality, and Long-term Exposure to Fine Particulate Air Pollution. JAMA 287, 1132–1141.
Reid, J.S., Xian, P., Hyer, E.J., Flatau, M.K., Ramirez, E.M., Turk, F.J., Sampson, C.R., Zhang, C., Fukada, E.M., Maloney, E.D., 2012. Multi-scale meteorological conceptual analysis of observed active fire hotspot activity and smoke optical depth in the Maritime Continent. Atmos. Chem. Phys. 12, 2117–2147.
Romanello, M., et al., 2022. The 2022 report of the Lancet Countdown on health and climate change: health at the mercy of fossil fuels. Lancet 400, 1619–1654.
Saji, N.H., Yamagata, T., 2003. Possible impacts of Indian Ocean Dipole mode events on global climate. Climate Res. 25, 151–169.
Pope, C.A., 2000. Epidemiology of fine particulate air pollution and human health: biologic mechanisms and who's at risk? Environ. Health Perspect. 108, 713–723.
Schiavina, M., Freire, S. & MacManus, K. GHS-POP R2019A - GHS population grid multitemporal (1975-1990-2000-2015) - OBSOLETE RELEASE. (2019) doi: 10.2905/0C6B9751-A71F-4062-830B-43C9F432370F.
Siegert, F., Ruecker, G., Hinrichs, A., Hoffmann, A.A., 2001. Increased damage from fires in logged forests during droughts caused by El Niño. Nature 414, 437–440.
Singh, G.M., et al., 2013. The Age-specific quantitative effects of metabolic risk factors on cardiovascular diseases and diabetes: a pooled analysis. PLoS One 8, e65174.
Stauffer, R.M., Thompson, A.M., Witte, J.C., 2018. Characterizing global ozonesonde profile variability from surface to the UT/LS WITH A CLUSTERING TECHNIQUe and MERRA-2 reanalysis. J. Geophys. Res. Atmos. 123, 6213–6229.
Tosca, M.G., Randerson, J.T., Zender, C.S., Nelson, D.L., Diner, D.J., Logan, J.A., 2011. Dynamics of fire plumes and smoke clouds associated with peat and deforestation fires in Indonesia. J. Geophys. Res: Atmos. 116.
van den Dool, H.M., Saha, S., Johansson, Å., 2000. Empirical orthogonal teleconnections. J. Clim. 13, 1421–1435.
Wu, W., Yao, M., Yang, X., Hopke, P.K., Choi, H., Qiao, X., Zhao, X., Zhang, J., 2021. Mortality burden attributable to long-term ambient PM2.5 exposure in China: using novel exposure-response functions with multiple exposure windows. Atmos. Environ. 246, 118098.
Yim, S.H.L., Barrett, S.R.H., 2012. Public health impacts of combustion emissions in the United Kingdom. Environ. Sci. Technol. 46, 4291–4296.
Yim, S.H.L., Hou, X., Guo, J., Yang, Y., 2019. Contribution of local emissions and transboundary air pollution to air quality in Hong Kong during El Niño-Southern Oscillation and heatwaves. Atmos. Res. 218, 50–58.